Lunar Noise-Temperature Increase Measurements at S-Band, X-Band, and Ka-Band Using a 34-Meter-Diameter Beam-Waveguide Antenna

D. D. Morabito[1]

The Moon radiates energy at infrared and microwave wavelengths, in addition to reflecting sunlight at optical wavelengths. As a result, an antenna pointed at or near the Moon will cause an increase in receiver noise temperature that needs to be accounted for in telemetry, radio science, or ranging link budgets. The Deep Space Network may be required to use its antennas in future lunar robotic or human missions, and thus it is important to understand the nature of this temperature increase as a function of observing frequency, lunar phase, and angular offset of the antenna beam from the center of the lunar disk. This article quantifies such a set of measurements acquired at DSS 13, a 34-m-diameter research and development beam-waveguide antenna located at Goldstone, California, at three different telecommunication frequencies, S-band (2.3 GHz), X-band (8.4 GHz) and Ka-band (32 GHz), over a wide range of lunar phase, for both disk-centered and limb-centered positions of the antenna beam.

I. Introduction

The Moon radiates energy at infrared and microwave wavelengths, in addition to the reflecting of sunlight at visible wavelengths. When one views the Moon, one perceives the light reflected from the Sun. This is manifested in the synodic lunar phase cycle that repeats as the Moon orbits the Earth relative to the direction of the Sun. This period of lunation or repetition of lunar phases occurs at the synodic period of about 29.5 days, a lunar month. At other wavelengths, there is very little reflected radiation, so the emission is dominated by thermal emission, which is related to the Moon's surface temperature, which in turn is related to the properties of the lunar surface material and the amount of sunlight incident upon it. For the Moon, the infrared emission variation is well correlated with the lunar phase cycle as it originates from a thin surface layer of the Moon.

However, at millimeter and centimeter radio wavelengths, the degree of this variation is much less than at infrared due to the fact that radio emission originates from some depth below the surface. The surface layers are heated by conduction, and thus the variations in the radio emission lag behind the

[1] Communications Architectures and Research Section.

The research described in this publication was carried out by the Jet Propulsion Laboratory, California Institute of Technology, under a contract with the National Aeronautics and Space Administration.

lunar phase cycle of solar heating. Hence, the longer the wavelength, the deeper the surface from which the radiation is emitted. The amplitude and phase of the variation is wavelength dependent, and the phase is consistent with that of the solar insolation. The degree of variation versus lunar phase observed for radio wavelengths longer than 5 cm is not significant. Thus, one would not expect any significant variation with lunar phase at S-band (13 cm), whereas one would expect progressively more variation from X-band (3.6 cm) to Ka-band (0.9 cm).

Because of the prospect of revisiting the Moon with future human and robotic expeditions, the realization of very high data rates requires a thorough understanding of all contributions in the link calculations. Among these contributions, the additional system noise-temperature increase while pointing a large-diameter antenna onto the disk of the moon must be characterized, either by modeling or by direct measurement. The potential of using the NASA Deep Space Network (DSN) 34-m beam-waveguide antennas to realize high data rates [1] merits investigating these temperature increases. This information is needed for communication links at different frequencies (S-band, X-band and Ka-band).

This article describes a measurement campaign undertaken at DSS 13, a 34-m-diameter research and development (R&D) beam-waveguide antenna located at the NASA Deep Space Communications Complex at Goldstone near Barstow, California. The system noise-temperature increases measured at S-band, X-band, and Ka-band can be used in telecommunications link budgets for future lunar and robotic missions. The increases in system noise temperature were measured at the center of the lunar disk (antenna beam Moon-centered), at the limb of the lunar disk (antenna beam moved one lunar radius off center in each direction parallel to the horizon), and relative to the background (antenna beam moved 5 deg off center in each direction). The statistics of the limb-centered measurements would be useful in planning communication links where the antenna beam is pointed at a lunar limb. An example of one such site would be Malapert Mountain in the southern lunar pole, which has been identified as a unique site to serve as a microwave relay station [2]. The focus of future measurement sessions would include taking noise-temperature increase measurements pointed at such specific sites, using the expected link frequencies.

Past work showed that radio observations of the Moon display a quasi-sinusoidal variation of brightness temperature with lunar phase about a mean brightness temperature. The amplitude and phase of this variation have a wavelength dependence [3] although at larger wavelengths above 5 cm the variation is small or nonexistent [4].

II. Calibration Measurements

The measurements were conducted at DSS 13, a beam-waveguide antenna that consists of a 34-m-diameter main reflector surface, main subreflector, and a series of reflectors and mirrors that guide the radiation down into a subterranean pedestal room, where a central ellipsoid mirror directs the energy to one of several feed packages situated in a concentric ring. The use of a subterranean room insulates the equipment from outside weather effects such as rain and wind as well as facilitating equipment maintenance.

Two of the feed packages utilized for this experiment are located at the S-/X-band feed position in the DSS-13 pedestal room, making use of an S-/X-band dichroic plate and S-band and X-band packages consisting of feed horns, low-noise amplifiers, and follow-on equipment. This allows for simultaneous reception of S-band and X-band signals. The X-/Ka-band position on the concentric ring makes use of an X-/Ka-band dichroic plate and X-band and Ka-band packages. This allows for simultaneous reception of X-band and Ka-band signals. The packages all include front-end low-noise amplifiers where high electron mobility transistors (HEMTs) are the active components. These packages also employ downconverter follow-on equipment and calibration hardware (noise diodes and ambient loads). A total power radiometer (TPR) is used to measure the system noise temperature and perform system calibrations. The center

frequencies were 2295 MHz for S-band, 8425 MHz for X-band (S-/X-band system), 8415 MHz for X-band (X-/Ka-band system), and 32,000 MHz for Ka-band. The specifics of each observing wavelength are provided in Table 1.

Prior to each pass, a sequence of calibrations, known as minicals, was performed [5]. Each minical measurement consists of measuring the received power while on (1) cold sky (zenith), (2) cold sky plus noise diode, (3) ambient load, and (4) ambient load plus noise diode. From these measurements, a calibration relating output power as measured by the power meter versus input noise temperature (calibrated with physical temperature) was performed, as well as characterization of the system linearity. Each minical takes about two minutes to complete. A series of six consecutive minicals for X-band and Ka-band is usually performed prior to the data acquisition at the X-/Ka-band feed position. A series of six consecutive minicals for S-band and X-band is usually performed prior to the data acquisition at the S-/X-band feed position.

Tables 2 through 5 summarize the calibrations for S-band (S-/X-band feed position), X-band (S-/X-band feed position), X-band (X-/Ka-band feed position), and Ka-band (X-/Ka-band feed position), respectively. For the purpose of characterizing the system and atmosphere for each pass, the zenith system noise temperature obtained from the minicals is listed along with its standard deviation over the period of the minicals. The average system noise temperature and its scatter while on the ambient load are also tabulated.

For the first few passes, the ambient load thermometer in the second package at each feed position was stuck on a canned-in value. To remedy this, the ambient load temperature used in the calibration was forced to match with that measured at the nearest other ambient load sensor in the pedestal room.

The system gain is determined using the ambient load, whose physical temperature is measured independently. In Tables 2 through 5, the relative fluctuations in the system gain over the period of the six minicals are reflected in the "Gain change, percent" columns, which provide a measure of how the system changes over the course of the 12-minute calibration measurement period. The linearity factor is a measure of how linear the calibrated system temperature versus measured noise power is over the four measurement points: (1) cold sky, (2) cold sky plus noise diode, (3) ambient load, and (4) ambient load plus noise diode.

System noise temperatures at zenith averaged 59.6 ± 2.6 K for the Ka-band system, 49.2 ± 0.5 K for the X-band system at the X-/Ka-band feed position, 43.8 ± 0.5 K for the X-band system at the S-/X-band feed position, and 37.4 ± 0.5 K for the S-band system. These measurements are long-term averages that include atmospheric variable effects (more significant at Ka-band), not just equipment noise.

Table 1. Observing-frequency specifications.

Band	Frequency, MHz	Bandwidth, MHz	Polarization	Feed package
S-band	2,295	20	LCP[a]	S-/X-band
X-band	8,425	20	LCP	S-/X-band
X-band	8,415	20	LCP	X-/Ka-band
Ka-band	32,000	30	RCP[b]	X-/Ka-band

[a] LCP = left circular polarization.

[b] RCP = right circular polarization.

Changes in gain measured over the minical period (several minutes) usually lie near or below 0.1 percent. During the lunar brightness temperature measurement period of about 1 hour, which follows the calibrations, the projected uncertainty due to gain variation is small (∼1 percent). The pedestal room is usually kept well controlled and isolated from the outside environmental changes, as can be inferred from the ambient load measurements in Tables 2 through 4 ($T_{\rm load}$ standard deviation column). In general, the system nonlinearity [$NL = 100 * (FL - 1)$, where FL is "linearity factor" in Tables 2 through 5] was excellent, lying below the −0.5 percent DSN requirement for the majority of the passes at S-band and X-band. At Ka-band, although the nonlinearity was generally higher, averaging about −1.8 percent, its measurement allows for correction of such effects.

Table 2. S-band calibration summary (S-/X-band feed position).

Year	Day	$T_{\rm zenith}$ average, K	$T_{\rm zenith}$ standard deviation, K	$T_{\rm load}$ average, K	$T_{\rm load}$ standard deviation, K	Linearity factor	Gain change, percent	Number of calibrations
2004	208	37.65	0.07	315.28	0.110	0.9965	0.06	8
2004	212	37.56	0.11	315.82	0.005	0.9990	0.25	5
2004	213	37.45	0.01	314.06	0.020	0.9965	0.05	6
2004	215	37.25	0.15	312.10	0.006	0.9931	0.28	5
2004	217	37.38	0.05	311.83	0.016	0.9968	0.08	6
2004	223	37.66	0.01	313.03	0.008	0.9961	0.05	4
2004	224	37.71	0.01	313.50	0.010	0.9962	0.02	4
2004	226	37.63	0.02	312.81	0.017	0.9979	0.24	8
2004	237	37.58	0.05	312.89	0.019	0.9954	0.27	6
2004	240	37.29	0.01	311.51	0.027	0.9969	0.05	6
2004	241	37.50	0.06	311.84	0.006	0.9941	0.18	6
2004	243	37.36	0.02	311.00	0.012	0.9965	0.04	6
2004	245	37.48	0.02	310.82	0.014	0.9964	0.08	6
2004	247	37.51	0.04	310.88	0.000	0.9966	0.11	6
2004	251	37.50	0.05	311.12	0.041	0.9969	0.09	12
2004	252	37.63	0.02	311.95	0.004	0.9963	0.07	6
2004	254	37.73	0.02	311.64	0.014	0.9975	0.04	6
2004	258	37.67	0.03	311.39	0.379	0.9970	1.09	7
2004	260	37.77	0.03	311.48	0.005	0.9963	0.09	6
2004	261	37.70	0.04	311.18	0.008	0.9960	0.11	6
2004	265	37.23	0.03	309.34	0.004	0.9966	0.07	6
2004	266	37.21	0.07	309.96	0.005	0.9964	0.04	6
2004	269	37.58	0.11	310.66	0.014	0.9973	0.08	6
2004	273	37.42	0.71	311.32	0.004	0.9991	0.13	6
2004	315	36.44	0.14	306.79	0.032	0.9980	0.46	7
2004	321	36.99	0.06	308.10	0.011	0.9969	0.17	6
2004	323	36.80	0.01	308.61	0.004	0.9961	0.04	6
2004	337	38.75	0.01	302.70	0.004	0.9973	0.02	6
2004	338	36.20	0.01	302.08	0.005	0.9971	0.02	6
2005	63	35.92	0.16	305.54	0.005	0.9995	0.11	7
	Average	37.38	0.07	310.44	0.03	0.997	0.147	6.2
	Sigma	0.52	0.13	3.51	0.07	0.001	0.204	—
Error in mean		0.10	—	0.64	—	—	0.04	—

Table 3. X-band calibration summary (S-/X-band feed position).

Year	Day	$T_{\rm zenith}$ average, K	$T_{\rm zenith}$ standard deviation, K	$T_{\rm load}$ average, K	$T_{\rm load}$ standard deviation, K	Linearity factor	Gain change, percent	Number of calibrations
2004	208	44.30	0.14	315.13	0.110	0.9980	0.28	8
2004	212	44.08	0.06	315.67	0.005	0.9972	0.09	5
2004	213	43.80	0.03	313.89	0.020	0.9975	0.12	6
2004	215	43.98	0.05	311.95	0.006	0.9965	0.10	5
2004	217	43.39	0.16	310.89	0.016	0.9966	0.38	6
2004	223	43.94	0.01	311.80	0.020	0.9958	0.03	4
2004	224	44.10	0.03	312.11	0.010	0.9950	0.13	4
2004	226	44.65	0.06	311.56	0.010	0.9976	0.07	8
2004	237	44.24	0.05	311.28	0.030	0.9965	0.07	6
2004	240	43.32	0.12	309.63	0.050	0.9961	0.30	6
2004	241	43.66	0.02	310.30	0.010	0.9976	0.09	6
2004	243	43.54	0.03	309.26	0.010	0.9963	0.15	6
2004	245	43.51	0.03	309.33	0.010	0.9965	0.11	6
2004	247	43.71	0.08	308.87	0.045	0.9974	0.17	6
2004	251	43.57	0.05	309.75	0.011	0.9960	0.07	6
2004	252	44.03	0.03	310.36	0.008	0.9966	0.07	6
2004	254	44.56	0.05	310.41	0.006	0.9962	0.08	6
2004	258	44.21	0.03	310.11	0.005	0.9957	0.10	6
2004	260	44.51	0.04	310.12	0.000	0.9944	0.07	6
2004	261	44.32	0.04	309.87	0.004	0.9948	0.19	6
2004	265	43.69	0.03	307.34	0.008	0.9958	0.07	6
2004	266	43.68	0.06	308.32	0.005	0.9953	0.08	6
2004	273	43.30	0.02	308.98	0.029	0.9966	0.06	6
2004	315	43.17	0.02	305.47	0.030	0.9959	0.70	7
2004	321	43.08	0.03	306.93	0.010	0.9961	0.06	6
2004	323	43.14	0.03	307.08	0.008	0.9952	0.06	6
2004	337	43.33	0.02	301.18	0.011	0.9943	0.05	6
2004	338	42.21	0.04	300.43	0.029	0.9936	0.07	6
2005	63	44.22	0.08	304.93	0.011	0.9936	0.06	7
	Average	43.77	0.05	309.41	0.020	0.9960	0.134	6
	Sigma	0.54	0.04	3.42	0.02	0.001	0.135	—
Error in mean		0.1	—	0.63	—	—	0.03	—

Table 4. X-band calibration summary (X-/Ka-band feed position).

Year	Day	T_{zenith} average, K	T_{zenith} standard deviation, K	T_{load} average, K	T_{load} standard deviation, K	Linearity factor	Gain change, percent	Number of calibrations
2004	208	50.09	0.03	320.93	0.04	0.9960	0.06	6
2004	212	50.04	0.06	321.54	0.32	0.9953	0.91	9
2004	213	49.80	0.13	320.00	0.44	0.9955	0.40	12
2004	215	49.56	0.05	317.22	0.02	0.9964	0.04	6
2004	217	49.24	0.05	317.00	0.03	0.9960	0.13	6
2004	223	49.08	0.14	314.79	1.00	0.9961	0.20	6
2004	224	49.10	0.04	314.94	0.01	0.9958	0.04	6
2004	226	49.64	0.05	314.70	0.01	0.9957	0.05	12
2004	236	49.75	0.04	315.29	0.02	0.9955	0.10	6
2004	240	49.67	0.04	314.40	0.01	0.9957	0.10	6
2004	241	49.61	0.02	313.96	0.00	0.9958	0.06	5
2004	243	49.09	0.01	312.84	0.01	0.9964	0.04	6
2004	245	48.88	0.05	310.32	0.04	0.9966	0.07	12
2004	247	48.80	0.04	313.06	0.01	0.9959	0.03	6
2004	251	48.50	0.03	312.50	0.03	0.9960	0.05	6
2004	252	48.78	0.05	313.67	0.02	0.9958	0.03	7
2004	254	49.25	0.03	312.89	0.02	0.9959	0.07	6
2004	258	49.18	0.04	313.55	0.01	0.9961	0.05	6
2004	260	49.16	0.04	313.26	0.01	0.9961	0.06	6
2004	261	49.03	0.03	313.94	0.00	0.9962	0.04	7
2004	265	48.77	0.02	311.12	0.01	0.9960	0.05	6
2004	266	48.83	0.02	311.86	0.01	0.9962	0.07	10
2004	269	49.00	0.04	313.04	0.04	0.9960	0.08	9
2004	274	49.00	0.49	312.09	0.04	0.9961	0.45	9
2004	321	48.88	0.05	310.32	0.04	0.9966	0.07	12
2004	323	48.96	0.02	310.58	0.01	0.9963	0.05	7
2004	337	48.99	0.89	304.80	0.01	0.9963	0.11	6
2004	338	48.13	0.19	303.88	0.00	0.9973	0.11	6
Average		49.17	0.10	313.52	0.08	0.9961	0.125	7.4
Sigma		0.46	0.18	3.88	0.21	0.0004	0.183	—
Error in mean		0.09	—	0.73	—	—	0.03	—

Table 5. Ka-band calibration summary (X-/Ka-band feed position).

Year	Day	T_{zenith} average, K	T_{zenith} standard deviation, K	T_{load} average, K	T_{load} standard deviation, K	Linearity factor	Gain change, percent	Number of calibrations
2004	208	57.49	0.059	318.64	0.06	0.9509	0.04	6
2004	212	59.17	0.058	330.14	—	0.9832	0.10	6
2004	213	57.47	0.135	328.44	—	0.9805	1.94	12
2004	215	61.17	0.044	325.66	—	0.9804	0.05	6
2004	217	57.93	0.069	325.44	—	0.9737	0.06	6
2004	223	60.50	0.118	326.83	1.12	0.9816	0.25	6
2004	224	60.90	0.027	326.88	0.02	0.9776	0.07	6
2004	226	70.30	1.466	326.69	0.07	0.9817	0.06	12
2004	237	58.95	0.136	326.95	0.01	0.9867	0.08	6
2004	240	58.33	0.040	326.24	0.02	0.9852	0.04	4
2004	241	59.49	0.032	325.70	0.01	0.9849	0.09	6
2004	243	59.20	0.046	324.68	0.02	0.9850	0.11	6
2004	245	59.43	0.173	322.58	0.03	0.9840	0.84	9
2004	247	57.22	0.100	325.02	0.01	0.9867	0.27	6
2004	251	57.64	0.047	324.89	0.02	0.9848	0.05	6
2004	252	59.47	0.081	325.78	0.01	0.9842	0.04	7
2004	254	63.88	0.125	324.85	0.03	0.9850	0.10	6
2004	258	58.92	0.019	325.41	0.01	0.9848	0.04	6
2004	260	59.54	0.242	324.97	0.02	0.9859	0.11	6
2004	261	58.12	0.152	324.77	0.01	0.9869	0.05	7
2004	265	58.47	0.044	322.90	0.03	0.9851	0.07	6
2004	266	59.90	0.050	323.63	0.01	0.9856	0.05	9
2004	274	60.65	2.310	323.95	0.17	0.9938	0.83	9
2004	321	59.43	0.173	322.58	0.03	0.9840	0.84	9
2004	323	59.58	0.012	323.63	0.02	0.9799	0.05	6
2004	337	59.65	2.360	316.98	0.05	0.9688	0.05	6
2004	338	56.06	0.246	316.14	0.02	0.9761	0.09	6
	Average	59.59	0.31	324.46	0.08	0.982	0.235	6.9
	Sigma	2.63	0.64	3.11	0.23	0.008	0.422	—
Error in mean		0.51	—	0.60	—	—	0.08	—

III. Disk-Centered Lunar Noise-Temperature Measurements

Unlike previous radio source noise-temperature measurement campaigns in which the radio source size usually was smaller than the main beam of the antenna [6], the Moon is an extended source whose apparent size is comparable to the main beam of the 34-m-diameter antenna at S-band and is significantly larger than the main beam and extent of the major side lobes at X-band and Ka-band (see Fig. 1).

Here we assumed that the antenna main beam was comparable to or smaller than the source size. The antenna was moved in cross-elevation angle, which is the direction across the source that is parallel to the horizon. This was done in order to minimize elevation-angle-dependent effects such as those due

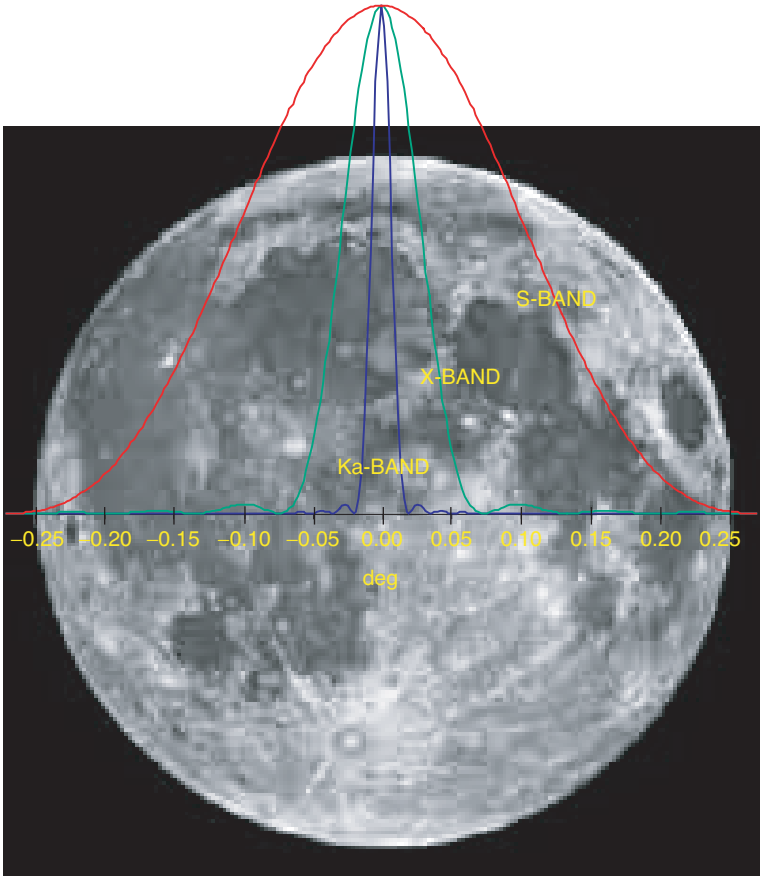

Fig. 1. Lunar disk with idealized one-dimensional beam patterns for a 34-m-diameter antenna at S-band (2295 MHz), X-band (8425 MHz), and Ka-band (32,000 MHz).

to atmosphere. The TPR was set to integrate and output 1 point every 1 second. Appropriate filters at the input to the power meters were used at each frequency band (see Table 1). The system noise temperature was measured using the TPR by pointing the antenna at one of the following positions for about 5 minutes:

- Off source in positive cross-elevation 5 deg
- On the lunar limb one lunar radius in positive cross-elevation
- Centered on the lunar center
- On the lunar limb one lunar radius in negative cross-elevation
- Off source in negative cross-elevation 5 deg

Examples of sequences of measurements are provided in Fig. 2 for S-band, Fig. 3 for X-band (S-/X-band position), Fig. 4 for X-band (X-/Ka-band position), and Fig. 5 for Ka-band.

In general, the measurement of the system noise-temperature (T_{op}) increase at an elevation angle θ is expressed as

$$\Delta T(\theta) = T_{\text{op,on-source}}(\theta) - T_{\text{op,off-source}}(\theta) \tag{1}$$

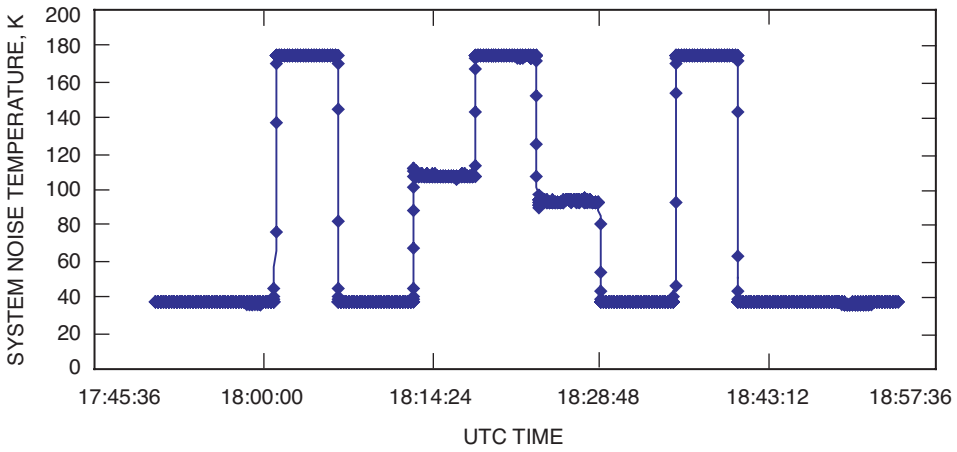

Fig. 2. S-band system noise-temperature measurements acquired on 2004/226 (S-/X-band feed position).

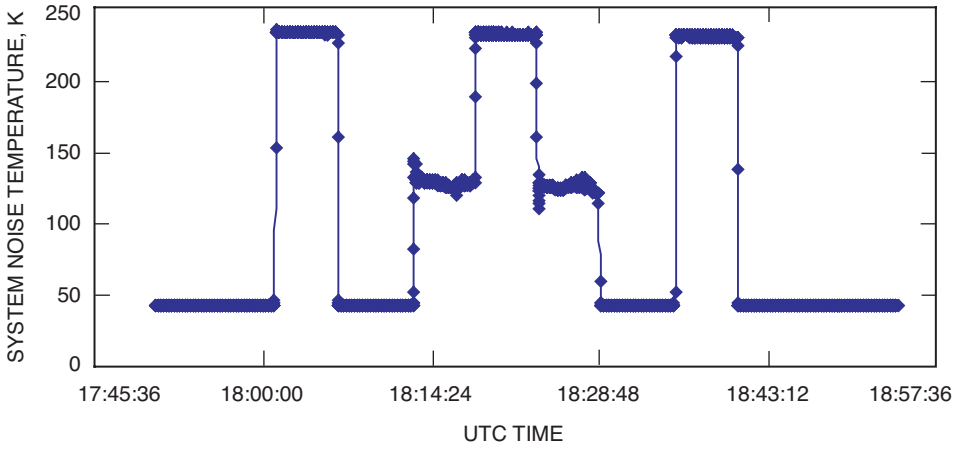

Fig. 3. X-band system noise-temperature measurements acquired on 2004/226 (S-/X-band feed position).

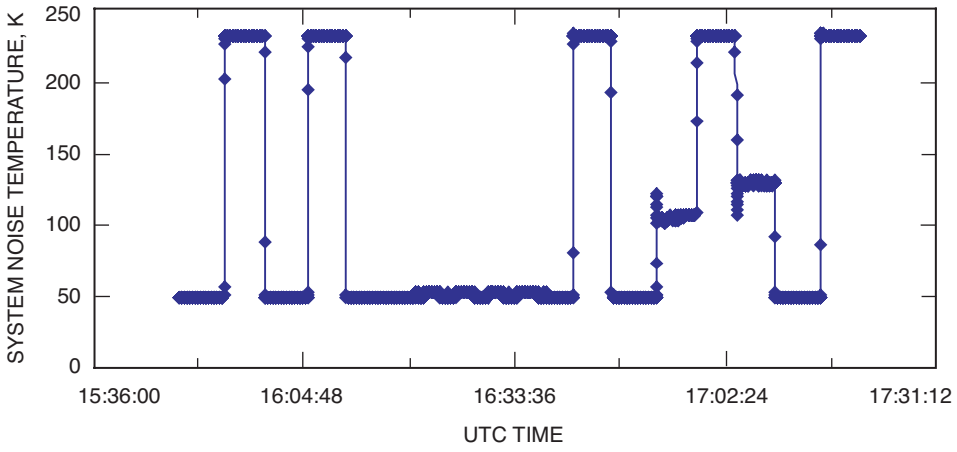

Fig. 4. X-band system noise-temperature measurements acquired on 2004/226 (X-/Ka-band feed position).

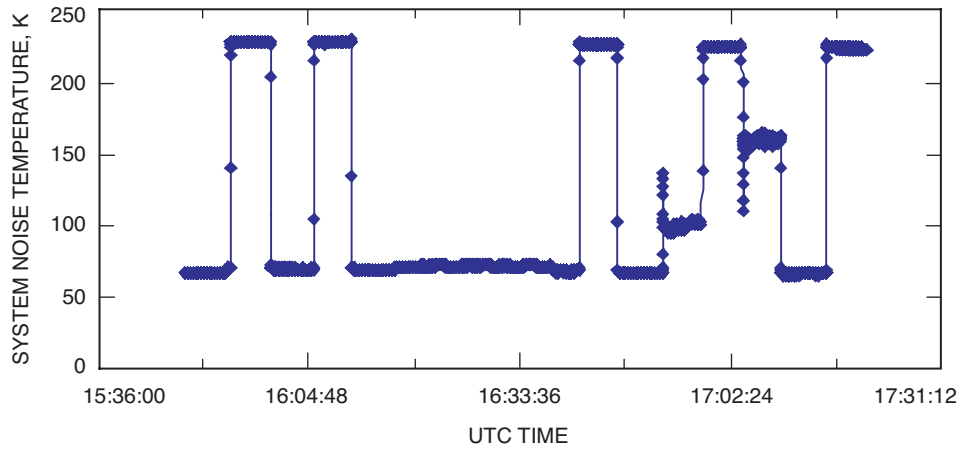

Fig. 5. Ka-band system noise-temperature measurements acquired on 2004/226 (X-/Ka-band feed position).

The measured system noise temperature increase for the disk-centered measurement is given by

$$\Delta T(\theta) = T_{\text{disk-centered}}(\theta) - T_{\text{off-source}}(\theta) \tag{2}$$

where the disk-centered and off-source values are averages over the measurement period for the respective positions. Because the measurement sequence is performed across a slice in cross-elevation, and repeated, the disk-centered and off-source measurements can be averaged, effectively removing elevation-angle dependence. The measurement sequence at the S-/X-band position consisted of five minutes each on the following:

- Zenith
- On source (disk centered)
- Off source +5 deg cross-elevation [azimuth $*$ cos (elevation)]
- Limb centered one lunar radius off center in the positive cross-elevation direction
- On source (disk centered)
- Limb centered one lunar radius off center in the negative cross-elevation direction
- Off source −5 deg cross-elevation
- On source (disk centered)
- Off source +5 deg cross-elevation
- Zenith

The measurement sequences for the X-/Ka-band feed position were conducted similarly but were preceded by peaking the antenna beam on an angularly nearby radio source. This allowed for offsets to the blind pointing model to be determined for use on centering the antenna beam on the limb of the Moon during the limb-centered measurements. Only one cycle of measurements was performed per pass.

The sequence of measurements at the X-/Ka-band position consisted of 5 minutes each on the following:

- Zenith
- On source (disk centered)
- Off source +5 deg cross-elevation [azimuth $*$ cos (elevation)]
- On source (disk centered)
- Off source −5 deg cross-elevation
- Autobores of natural radio source (about one-half hour)
- On source (disk centered)
- Off source +5 deg cross-elevation
- Limb centered one lunar radius off center in the positive cross-elevation direction
- On source (disk centered)
- Limb centered one lunar radius off center in the negative cross-elevation direction
- Off source −5 deg cross-elevation
- On source (disk centered)

A sequence of autobores on a nearby natural radio source is performed prior to the set of measurements that includes limb-centered measurements, so that the best available pointing offsets in elevation and cross-elevation relative to the blind pointing model are used. This is especially critical for Ka-band, where the half-power beamwidth for the 34-m-diameter antenna is about 18 mdeg (end-to-end) and the blind pointing model of the antenna in the ecliptic region is believed to be accurate to about 5 to 10 mdeg. The proximity of the radio source is also important, as the nearer it is to the Moon (in angle), the more precise the pointing correction will become. The autobores are intended to reduce the pointing error, which is especially critical at Ka-band for the limb-centered observations.

An average of the disk-centered measurements is taken as well as averages of the off-source measurements (in positive and negative cross-elevation directions). The averages are differenced to get the resulting system noise-temperature increase due to the Moon. The differences between on-source (disk-centered) and off-source (5 deg away from lunar disk center) are tabulated in Table 6. The averages and standard deviations of this difference provide information on its variability with lunar phase.

The average S-band value of 135.9 ± 1.4 K exhibits very little variation, about 1 percent. The average X-band value of $\sim 189.1 \pm 5.5$ K at the S-/X-band package exhibits 3 percent variation. The average Ka-band value of 166 ± 20 K exhibits significantly more variation, as expected, at the smaller wavelength, about 12 percent. Note that S-band (13-cm wavelength) exhibits the smallest variation of about 1 percent, whereas X-band (3.6-cm wavelength) exhibits a variation of about 3 percent, and Ka-band (0.94 cm) exhibits the highest variation of about 12 percent. These variations in measured noise-temperature increase are consistent with expected levels based on previous studies on lunar brightness temperatures [3,4].

These disk-centered values would be useful in telemetry link budgets while an antenna is pointed on the surface of the Moon. As the beam is moved off center, the brightness temperature is usually expected to decrease across the lunar disk, becoming significantly smaller at the lunar limb. Thus, these numbers can be considered conservative values. It is recommended one use the peak noise-temperature increase during the lunar cycle for simplicity if a lunar phase variation model is not yet practical to implement. A graphical representation of the system noise-temperature increase as a function of lunar phase is displayed in Fig. 6(a) for the two X-band packages and Fig. 6(b) for the S-band and Ka-band packages. This information then can be directly used in link calculations using a 34-m-diameter antenna, when

Table 6. System noise-temperature increase, Moon-centered.

Date, m/d/y	Day	UTC time, h:min	Mean elevation, deg	Illuminated fraction	Lunar phase, deg	ΔT S-band (S/X), K	ΔT X-band (S/X), K	UTC time, h:min	Mean elevation, deg	ΔT X-band (X/Ka), K	ΔT Ka-band (X/Ka), K
05/27/04	148	22:36	29.9	0.57	102.6	135.5	183.3	21:50	21.1	—	143.5
07/27/04	209	1:40	27.7	0.71	127.8	135.6	176.5	23:50	15.3	178.92	139.2
07/30/04	212	4:43	22.3	0.96	172.8	136.39	186.5	3:18	13.3	185.67	164.79
07/31/04	213	6:43	28.1	0.994	178.92	137.38	192.0	5:20	21.7	186.4	181.23
08/02/04	215	13:33	14.5	0.96	187.2	134.68	192.1	12:06	28.2	193.27	182.29
08/04/04	217	15:20	21.1	0.82	212.4	136.46	192.56	13:57	35.9	195.1	187.5
08/10/04	223	17:51	60.67	0.251	314.82	137.9	186.57	16:04	79.3	187.2	163.16
08/11/04	224	17:34	74.16	0.17	329.4	136.51	188.11	16:24	82.04	186.39	159.22
08/13/04	226	18:24	80.00	0.052	350.64	137.04	187.93	16:39	68.58	182.12	157.14
08/18/04	231	22:14	56.61	0.084	15.12	138.58	184.97	20:50	53.27	181.28	147.37
08/23/04	237	2:00	28.9	0.57	102.6	133.99	186.73	0:26	24.8	175.9	142.3
08/27/04	240	4:40	27.1	0.884	159.12	136.12	189.99	3:39	23.66	179.19	175.25
08/28/04	241	5:01	28.51	0.949	170.82	134.83	195.18	3:09	16.59	180.81	168.07
08/30/04	243	10:24	39.76	0.998	179.64	137.63	197.62	9:21	39.76	189.65	191.86
09/01/04	245	14:10	20.65	0.929	192.78	135.41	197.92	13:10	31.87	189.55	196.25
09/03/04	247	15:28	29.7	0.782	219.24	136.41	198.37	14:26	41.8	189.06	200.42
09/07/04	251	18:13	41.49	0.41	286.2	135.03	193.24	16:49	58.18	187.88	172.36
09/08/04	252	18:06	53.15	0.32	302.4	135.01	192.37	17:00	66.26	187.26	169.94
09/10/04	254	18:06	70.97	0.15	333	137.24	189.49	17:03	78.77	188.54	150.46
09/14/04	258	23:11	35.92	0.002	0.36	137.22	187.62	22:09	46.64	182.26	155.45
09/16/04	260	23:06	40.12	0.063	11.34	137.06	185.62	22:05	45.01	179.42	150.82
09/17/04	261	22:13	39.78	0.127	22.86	137.47	184.7	21:10	37.74	180.56	150.06
09/20/04	265	1:30	26.51	0.43	77.4	133.26	182.52	0:26	26.34	176.19	144.56
09/22/04	267	3:37	26.46	0.67	120.6	134.84	183.81	2:31	26.18	177.58	150.09
09/25/04	269	4:29	33.43	0.86	154.8	136.61	—	3:30	29.73	181.26	—
09/30/04	273	2:42	8.50	0.965	173.7	134.5	192.8	—	—	—	—
10/01/04	274	—	15.90	0.918	194.76	—	—	3:46	15.9	185.2	181.3
11/09/04	315	17:45	32.45	0.103	341.46	136.9	185.1	—	—	—	—
11/17/04	322	0:31	27.11	0.253	45.54	134.29	183.01	23:29	27.24	177.03	—
11/18/04	323	1:23	30.9	0.36	64.8	134.3	182.89	0:20	30.52	176.17	132.74
12/02/04	337	16:37	30.93	0.73	228.6	134.84	197.35	15:38	42.76	191.54	193.04
12/03/04	338	18:41	12.88	0.64	244.8	133.45	191	17:02	32.67	190.92	188.4
03/04/05	63	16:50	19.00	0.4	288	137.55	193.44	—	—	—	—
					Average	135.9	189.1			184.2	165.7
					Standard deviation	1.4	5.4			5.6	19.5
					Variation percent	1.0	2.8			3.0	11.8

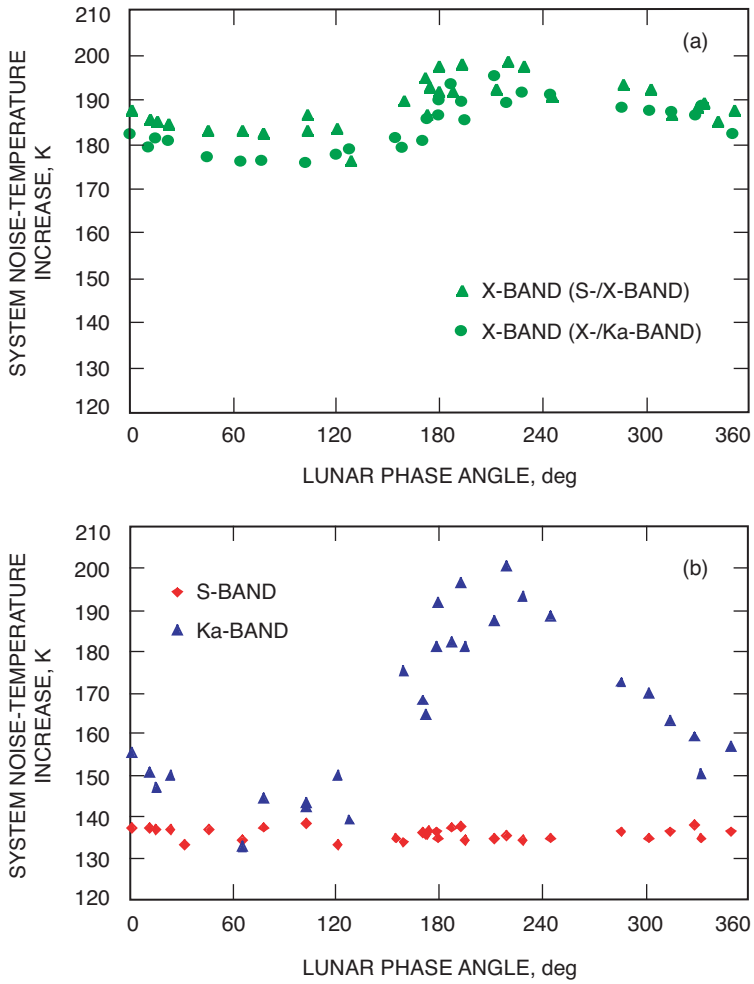

Fig. 6. Measured system noise-temperature increase of the 34-m-diameter BWG antenna, DSS 13 (antenna beam centered on lunar disk), as a function of lunar phase (0 deg = new moon, 180 deg = full moon): (a) X-band and (b) S-band and Ka-band.

the antenna beam is centered on the lunar disk. For the current measurement campaign status, Table 6 displays nominal averages acquired for measurement passes that are reasonably distributed over a lunar phase cycle. To obtain estimates of lunar brightness temperature, the measured system noise temperature differences have to be corrected for atmospheric attenuation (which varies with elevation angle), any system non-linearity, and antenna efficiency, including beam position considerations. In a future article, the conversion of these measurements into estimates of lunar brightness temperatures, their comparison with theory and other measurements, and subtleties of calculating efficiency for a large 34-m-diameter BWG antenna over an extended source will be addressed.

The X-band noise-temperature increase measurements acquired using the X-band package at the X-/Ka-band feed position (average 184.2 ± 5.6 K) are statistically consistent with those measured at the X-band package at the S-/X-band feed position (average 189.1 ± 5.4 K), but with a bias of about 4.9 K. The X-band data from the S-/X-band position being biased above those from the X-/Ka-band feed position [see Fig. 6(a)] may be indicative of feed package alignment issues at the X-/Ka-band position. The differences between the lunar noise-temperature estimates from the two X-band packages do

not show any significant variation with lunar phase. There is, however, a suggestion of variation in the difference-temperature increase as a function of elevation angle.

For telecommunications link calculations, the following models for system noise-temperature increase as a function of lunar phase angle, ϕ in degrees, are recommended. The lunar phase angle will lie below 180 deg while the phase of the Moon is waxing (new moon to full moon) and will lie above 180 deg while the lunar phase is waning (full moon to new moon).

S-band: $\Delta T(\phi) =$ 136 K for all ϕ with 1.4 K root-mean-square (rms) scatter

X-band: $\Delta T(\phi) = 189.1 - 0.31796\phi + 3.77896 \times 10^{-3}\phi^2 - 1.30776 \times 10^{-5}\phi^3 + 1.37099 \times 10^{-8}\phi^4$ with 3 K rms scatter

Ka-band: $\Delta T(\phi) = 154.0 - 0.14389\phi - 7.55628 \times 10^{-3}\phi^2 + 1.19848 \times 10^{-4}\phi^3 - 4.95709 \times 10^{-7}\phi^4 + 6.24376 \times 10^{-10}\phi^5$ with 6 K rms scatter

It is cautioned that these models are valid for the frequencies in the deep-space allocations for which the data were acquired. The downlink frequencies used in near-Earth allocations are close enough to those of the deep-space allocations such that the S-band and X-band models are not expected to differ significantly from the above. The near-Earth Ka-band allocation at 26.5 GHz will require a scaling from the deep-space 32-GHz Ka-band model above and, eventually, may require an independent set of measurements at 26.5 GHz.

In order to validate the disk-centered noise temperature increase measurements at all three frequency bands, a physical optics treatment of the problem was initiated, and the results are reported elsewhere in this issue [7].

IV. Limb-Centered Lunar Noise-Temperature Measurements

The measurements of the brightness temperature of the Moon with the antenna beam centered on the lunar limb are more difficult to characterize since the antenna beam is integrated over both lunar surface and cold sky. In addition, the brightness temperature of the surface near the limb is expected to be less than that at the disk center because the emissions in the direction of the Earth are only from those rays emanating from the limb, where a good fraction of the emission is emitted perpendicularly to the surface away from the Earth direction. The measurements are not expected to be symmetric between positive and negative cross-elevation angle offsets a lunar radius away because the illumination on each side may be different depending upon lunar phase, the lunar terrain being sampled, and possible mispointing of the antenna beam center. The uncertainty of the blind pointing model at different positions in the sky (especially significant at Ka-band) was minimized by performing a boresight observation on an angularly nearby radio source prior to the limb-centered measurements and using the corrected offsets while lunar tracking. The measurements taken at the two X-band systems are not expected to agree since they were acquired at different times, and their antenna pattern responses over the lunar disk and background cold sky probably would differ. A summary of the system noise-temperature increase measured during these passes at the S-/X-band feed position is presented in Table 7. The summary for the X-/Ka-band feed position is displayed in Table 8. The relevant statistics are presented at the bottom of each table.

No attempt was made to convert these measurements of noise-temperature increase into lunar brightness temperatures. They are intended to be used solely for future lunar link calculations using a 34-m-diameter antenna whose antenna pattern is peaked on the lunar limb, such as may be the case for communicating with lunar outposts such as those on Malapert Mountain near the south lunar pole [2].

A significant decrease in lunar brightness temperature is expected as the beam moves from disk center to the limb. In addition, the beam of the antenna is asymmetric and can pick up differing contributions of the lunar disk depending upon antenna beam orientation and lunar phase (whether the limb is illuminated or not).

Table 7. System noise-temperature increase, limb-centered using the S-/X-band system.

Year	Day	UTC time, h:min	Mean elevation, deg	Lunar phase, fraction	Lunar phase, deg	ΔT S-band (S/X) XEL+	ΔT S-band (S/X) XEL−	ΔT X-band (S/X) XEL+	ΔT X-band (S/X) XEL−
2004	148	22:36	29.9	0.57	102.6	—	—	—	—
2004	209	1:40	27.7	0.71	127.8	70.00	52.00	95.00	50.00
2004	212	4:43	22.3	0.96	172.8	73.62	53.34	110.46	51.59
2004	213	6:43	28.1	0.99	178.9	76.43	50.53	115.20	45.37
2004	215	13:33	14.5	0.96	187.2	52.66	50.83	50.32	54.84
2004	217	15:20	21.1	0.82	212.4	63.63	45.17	84.07	37.69
2004	223	17:51	60.7	0.25	314.8	63.22	45.52	57.51	50.80
2004	224	17:34	74.2	0.17	329.4	70.68	48.00	79.34	63.40
2004	226	18:24	80.0	0.05	350.6	70.70	56.27	84.7	82.09
2004	231	22:14	56.6	0.08	15.1	74.76	55.84	68.22	70.22
2004	237	2:00	28.9	0.57	102.6	70.60	54.10	61.78	66.36
2004	240	4:40	27.1	0.88	159.1	75.64	51.38	68.85	50.19
2004	241	5:01	28.5	0.95	170.8	69.89	56.13	98.71	71.19
2004	243	10:24	39.8	1.00	179.6	64.05	54.58	71.59	74.04
2004	247	15:28	29.7	0.78	219.2	67.87	42.92	97.47	34.14
2004	251	18:13	41.5	0.41	286.2	66.08	46.04	84.55	49.84
2004	252	18:06	53.2	0.32	302.4	70.07	45.24	91.79	50.90
2004	254	18:06	71.0	0.15	333.0	71.52	52.35	80.31	76.41
2004	258	23:10	35.9	0.00	0.4	68.65	55.18	87.66	69.42
2004	260	23:00	40.6	0.06	10.8	69.73	56.06	82.76	74.94
2004	261	22:09	—	0.13	22.9	70.85	56.12	89.67	70.79
2004	269	4:21	33.4	0.86	154.8	68.88	57.56	91.89	84.44
2004	322	0:27	27.1	0.25	45.5	70.23	54.77	93.05	66.34
2004	323	1:19	31.0	0.36	64.8	69.84	54.47	92.64	66.65
2004	337	16:38	30.7	0.73	228.6	60.93	53.77	71.23	74.55
2004	338	18:36	13.9	0.64	244.8	57.17	56.97	69.45	77.51
2005	63	16:36	20.3	0.40	288.0	66.92	71.25	78.57	80.11
					Mean	68.25	52.94	82.95	63.22
					Scatter	5.43	5.65	15.35	14.06
					Variation %	7.95	10.7	18.51	22.2
					Maximum	76.43	71.25	115.20	84.44
					Minimum	52.66	42.92	50.32	34.14

Table 8. System noise-temperature increase, limb-centered using the X-/Ka-band system.

Year	Day	UTC time, h:min	Mean elevation, deg	Lunar phase, fraction	Lunar phase, deg	ΔT X-band (X/Ka) XEL+	ΔT X-band (X/Ka) XEL−	ΔT Ka-band (X/Ka) XEL+	ΔT Ka-band (X/Ka) XEL−
2004	148	21:50	21.1	0.57	102.6	—	—	—	—
2004	209	23:50	15.3	0.71	127.8	99.53	45.63	44.54	50.29
2004	212	3:18	13.3	0.96	172.8	99.34	55.13	36.19	81.87
2004	213	5:20	21.7	0.994	178.92	134.72	29.69	137.56	21.89
2004	215	12:06	28.2	0.96	187.2	69.72	45.12	46.99	30.45
2004	217	13:57	35.9	0.82	212.4	96.24	32.67	111.66	16.89
2004	223	16:04	79.3	0.251	314.82	86.76	42.73	30.10	54.4
2004	224	16:24	82.04	0.17	329.4	103.47	56.04	48.56	92.75
2004	226	16:39	68.58	0.052	350.64	55.72	79.31	31.87	90.95
2004	231	20:50	53.27	0.084	15.12	111.27	51.84	85.02	73.97
2004	237	0:26	24.8	0.57	102.6	122.14	33.93	115.66	27.88
2004	240	3:39	23.66	0.884	159.12	114.84	32.55	100.17	28.21
2004	241	3:09	16.59	0.949	170.82	99.08	41.27	51.64	44.59
2004	243	9:21	39.76	0.998	179.64	92.19	61.91	45.91	103.08
2004	247	14:26	41.8	0.782	219.24	97.44	33.96	128.97	15.95
2004	251	16:49	58.18	0.41	286.2	90.92	44.03	103.34	20.05
2004	252	17:00	66.26	0.32	302.4	96.18	44.62	94.41	32.63
2004	254	17:03	78.77	0.15	333	94.70	70.82	32.27	124.07
2004	258	22:09	46.64	0.002	0.36	89.07	64.3	53.94	80.14
2004	260	22:05	45.01	0.06	10.8	90.14	64.72	35.40	105.62
2004	261	21:10	—	0.127	22.86	92.98	59.4	46.62	93.39
2004	269	—	—	0.86	154.8	—	—	—	—
2004	321	23:30	27.3	0.253	45.54	102.32	52.5	68.02	82.78
2004	323	0:20	30.5	0.36	64.8	106.24	50.12	62.18	65.9
2004	337	15:33	43.77	0.73	228.6	83.80	62.22	100.9	36.4
2004	338	17:26	27.84	0.64	244.8	69.23	80.12	80.46	68.17
					Mean	95.75	51.44	70.52	60.10
					Scatter	16.68	14.43	33.62	32.52
					Variation %	17.42	28.1	47.68	54.1
					Maximum	134.72	80.12	137.56	124.07
					Minimum	55.72	29.69	30.10	15.95

Figure 7 graphically displays averages of the differences between positive and negative cross-elevation (XEL) measurements of the lunar limbs for each 60-deg-wide bin of lunar phase. A significant bias apparently is favoring the positive cross-elevation direction for almost all data. The phase angle for each bin in Fig. 7 is not centered because it pertains to the average of the phase angles of the measurements in each bin.

One recommended way to use the data in Tables 7 and 8 for telecommunications link calculations when tracking an asset near the limb of the Moon would be to use the maximum values given in the statistical summary at the bottom of each table. This would provide a conservative worst-case design point. Another approach would be to use the mean values and their standard deviations in link budget tools that employ specific statistical distributions (using the means with favorable and adverse tolerances).

The averages of the means of the positive and negative cross-elevation limb-centered measurements provided at the bottom of Tables 7 and 8 run about 45 percent of the mean disk-centered S-band noise temperature (135.9 K) from Table 6. For the two X-band packages and the Ka-band package, the means of the positive and negative limb-centered measurements from the bottom of Tables 7 and 8 run about 40 percent of the mean disk-centered values of Table 6.

The asymmetry between the positive and negative cross-elevation-angle measurements averaged over all lunar phases likely is due to differences of illumination at each beam offset and possibly to differences in the terrain of the Moon that is sampled by the antenna beam at these two locations. Darker terrain is expected to be generally hotter than lighter terrain. This observed asymmetry is consistent with lunar brightness temperature maps[2] that were made available at these frequencies. Converting the noise temperature measurements to brightness temperatures and performing a detailed comparison with the brightness temperature maps is a focus of future study.

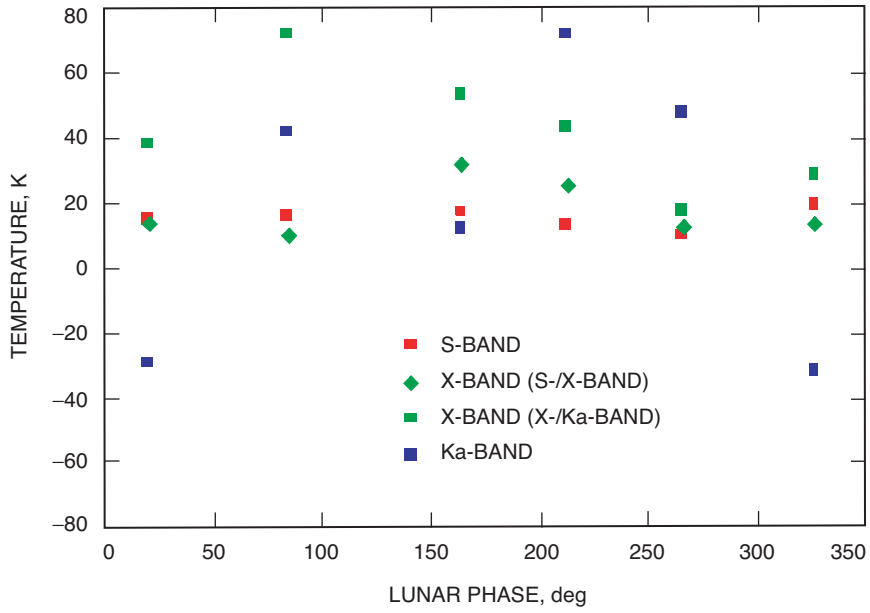

Fig. 7. Means of ΔT_{op} (XEL = +0.26 deg) – ΔT_{op} (XEL = –0.26 deg) for each 60-deg-wide bin of lunar phase.

[2] S. Keihm, personal communication, Jet Propulsion Laboratory, Pasadena, California, February 18, 2005.

V. Conclusion

The Moon radiates energy at infrared and microwave wavelengths, in addition to the reflecting of sunlight at visible wavelengths. As a result, an antenna pointed at or near the Moon will cause an increase in receiver noise temperature, which needs to be accounted for in link calculations used for for telemetry, radio science, or ranging. The Deep Space Network may be required to use its antennas in any future lunar robotic or human missions, and thus it is important to understand the nature of this temperature increase as a function of observing frequency, lunar phase, and angular offset from the center of the lunar disk. This article quantifies such a set of measurements recorded at DSS 13, a 34-m-diameter beam-waveguide antenna located at Goldstone, California, at three different telecommunication frequencies (S-band, X-band, and Ka-band), over a wide range of lunar phases, for both disk-centered and limb-centered positions of the antenna beam.

Measurements of system noise-temperature increase at the lunar limb would be useful in telecommunication link studies when tracking an asset near the lunar limb, such as at Malapert Mountain near the southern pole of the Moon.

Acknowledgments

The expertise and comments of several people are very much appreciated, including Steve Keihm, Charles Naudet, Watt Veruttipong, Charles Stelzried, Steven Slobin, Anil Kantak, William Imbriale, and Chi-Wung Lau. The support of Robert Cesarone and Rolf Hastrup is very much appreciated. The support of the DSS-13 staff also is very much appreciated, especially Ron Littlefair for generating script files to automate the measurement sequence.

References

[1] G. Noreen, R. Cesarone, L. Deutsch, C. Edwards, T. Ely, B. Cook, D. Morabito, H. Hemmati, S. Piazzolla, R. Hastrup, D. Abraham, M. Sue, and F. Manshadi, "Integrated Network Architecture for Sustained Human and Robotic Exploration," *Proceedings of the 2005 IEEE Aerospace Conference*, Big Sky, Montana, March 2005.

[2] B. L. Sharpe and D. G. Schrunk, "Malapert Mountain: Gateway to the Moon," *Adv. Space Res.*, vol. 31, no. 11, pp. 2467–2472, 2003.

[3] D. O. Muhleman, "Microwave Emission from the Moon," *Thermal Characteristics of the Moon*, J. W. Lucas, ed., *Progress in Astronautics and Aeronautics*, vol. 28, Cambridge, Massachusetts: The MIT Press, 1972.

[4] J. Kraus, *Radio Astronomy*, McGraw-Hill, 1966.

[5] C. Stelzried and M. Klein, "Precision DSN Radiometer Systems: Impact on Microwave Calibrations," *Proc. of the IEEE*, vol. 82, pp. 776–787, May 1994.

[6] D. D. Morabito, "The Characterization of a 34-Meter Beam-Waveguide Antenna at Ka-band (32 GHz) and X-band (8.4 GHz)," *IEEE Antennas and Propagation Magazine*, vol. 41, no. 4, pp. 23–34, August 1999.

[7] W. A. Imbriale, "Computing the Noise Temperature Increase Caused by Pointing DSS 13 at the Center of the Moon," *The Interplanetary Network Progress Report*, vol. 42-166, Jet Propulsion Laboratory, Pasadena, California, pp. 1–10, August 15, 2006. http://ipnpr/progress_report/42-166/166E.pdf